Eur. J. Mech. B - Fluids 20 (2001) 127–144
© 2001 Éditions scientifiques et médicales Elsevier SAS. All rights reserved
S0997-7546(00)01107-9/FLA

On the absolute instability in a boundary-layer flow with compliant coatings

Olivier Wiplier [a], Uwe Ehrenstein [b,*]

[a] *Laboratoire de Mécanique de Lille, Université de Lille 1, Bd. P. Langevin, 59655 Villeneuve d'Ascq cedex, France*
[b] *Laboratoire J.-A. Dieudonné, Université de Nice-Sophia Antipolis, Parc Valrose, 06108 Nice cedex 2, France*

(Received 8 February 2000; revised 19 June 2000; accepted 13 July 2000)

Abstract – The question of absolute instabilities occuring in a boundary-layer flow with compliant coatings is reassessed. Compliant coatings of the Kramer's type are considered. Performing a local, linear absolute/convective stability analysis, a family of spring-backed elastic plates with damping is shown to be absolutely unstable for sufficiently thin plates. The absolute instability arises from the coalescence between an upstream propagating evanescent mode and the Tollmien–Schlichting wave. To reinforce the local, linear stability results the global stability behaviour of the system is investigated, integrating numerically the full nonparallel and nonlinear two-dimensional Navier–Stokes system coupled to the dynamical model. Injecting Gaussian-type, spatially localized flow disturbances as initial conditions, the spatio-temporal evolution of wave packets is computed. The absolute stability behaviour is retrieved in the global system, for a compliant panel of finite length. It is demonstrated numerically that the global stability behaviour of the wall, triggered by finite-end-effects, may be independent of the disturbance propagation in the flow. © 2001 Éditions scientifiques et médicales Elsevier SAS

boundary-layer flow / compliant walls / absolute / convective instabilities

1. Introduction

Numerous investigations have been devoted to the analysis of the interaction between an unstable boundary-layer flow and a compliant coating. A quite recent review on the topic has been given by Gad-el-Hak [1]. Soon it has been recognized that compliant walls may be responsible for the occurrence of other instability mechanisms than the usual Tollmien–Schlichting waves which trigger the onset of transition in boundary-layer flows along rigid walls. According to a commonly used classification scheme (Carpenter and Garrad [2,3], the instability waves are divided into fluid-based Tollmien–Schlichting instabilities and solid-based flow-induced surface instabilities. The latter ones are analogous to instabilities observed in hydro- and aeroelasticity. They consist of travelling-wave flutter moving at speeds close to the solid free-wave-speed, as well as static, divergence waves. Thorough investigations of the influence of compliant coatings on Tollmien–Schlichting waves as well as the linear stability analysis of flow-induced surface instabilities are available since the work of Carpenter and Garrad [2,3]. The problem of the proper choice of coating parameters capable of delaying spatial instabilities has been addressed for instance by Joslin and Morris [4], and detailed studies of the influence of compliant coatings on secondary instabilities have been carried out (Joslin and Morris [5]). Most of the investigations available are based on linear temporal or spatial stability analyses using a locally-parallel flow assumption. The influence of the boundary-layer growth in the presence of compliant coatings has been addressed by Yeo et al. [6] using a multiple-scale analysis. Computing nonlinear travelling waves bifurcating at criticality in a Blasius boundary-layer flow, there is some evidence that the locally-parallel flow assumption is no longer relevant for highly compliant walls (Ehrenstein and Rossi [7]).

* Correspondence and reprints.
E-mail address: uwe.ehrenstein@unice.fr (U. Ehrenstein)

Investigating the stability behaviour of a boundary-layer flow bounded by a compliant wall in view of transition control (Gad-el-Hak [1]), most of the studies have focused on convective (spatial) instabilities. Using uniform potentiel flow, and performing a time-asymptotic analysis of spatio-temporal disturbances (Huerre and Monkewitz [8]), Brazier-Smith and Scott [9] have shown however that absolute instabilites may occur in flows bounded by compliant plates. Concerning Blasius boundary-layer flow Carpenter and Garrad [3] suggested that static divergence waves may be interpreted as absolute instabilities (see also the review of Carpenter [10]). Simulating the interaction of a compliant wall of finite length and unsteady potential flow an absolute-type stability behaviour has been demonstrated by Lucey and Carpenter [11]. More recently Lingwood and Peake [12] considered more realistic shear profiles, ranging from uniform flow, previously considered by Crighton and Oswell [13], to the Blasius profile. Focusing on local properties of the dispersion relation for the linearized Euler equations, Lingwood and Peake show in particular that the critical flow velocities for absolute instability depend strongly on the characteristic transverse length scale.

Considering viscoelastic damped walls, a systematic analysis of the dispersion relation with regard to absolute instability has been performed by Yeo et al. [14] for viscous boundary-layer flow. It is shown that absolute instabilities occur for large parameter ranges in both the Reynolds number and wall characteristics. Pinch-point singularities in the complex frequency-wavenumber dispersion relation have also been detected for instance in rotating-disc boundary-layer flow over compliant coatings (Cooper and Carpenter [15]). Hence, absolute instability behaviour is a general feature when fluid flow is bounded by elastic materials including for instance fluid-conveying flexural pipes (de Langre and Ouvrard [16]).

The aim of the present work is to reassess the question of absolute instability in a boundary-layer flow bounded by an elastic plate. Similar to Yeo et al.'s [14] analysis for viscoelastic walls, the dispersion relation for a boundary-layer flow over a damped, spring-backed elastic plate is analysed with regard to the existence of pinch-point singularities. The local analysis is reinforced solving the Navier–Stokes system coupled to the dynamical model. The global spatial evolution of wave packets is computed, starting from a Gaussian-type initial flow disturbance.

In section 2 we briefly recall the underlying computational model of our analysis as well as the numerical solution procedure used to solve the fluid-structure system (more details about the numerical method and the validation of the procedure may be found in Wiplier and Ehrenstein [17]). In section 3 we briefly survey the different spatial instability modes existing in a (convectively) unstable boundary-layer over a compliant wall, for the example of a spring-backed elastic plate. In section 4 a local linear stability analysis is first performed for complex frequencies and wavenumbers. It is shown that for sufficiently thin compliant panels with damping an evanescent mode and a Tollmien–Schlichting mode merge in the complex wavenumber plane for positive imaginary parts of the frequency, leading to absolute instability. The numerical simulation procedure is then used to simulate the spatial (nonparallel and nonlinear) evolution of wave packets triggered by a spatially localized initial condition. It is shown, how the trailing edge of the compliant panel generates the upstream propagating evanescent mode which coalesces in the absolutely unstable case with the travelling-wave-type Tollmien–Schlichting mode, leading to a rapid increase in perturbation amplitude. Finally, some conclusions are drawn in section 5.

2. Computational model

In this section the governing equations and the procedure capable of solving numerically the global fluid-structure system are briefly described. A complete analysis of the computational model may be found in Wiplier and Ehrenstein [17].

2.1. Wall model and basic state

We consider an incompressible fluid flow of viscosity ν^* past a plane wall, which in the rigid case is located at $y^* = 0$, $0 \leqslant x^*$. The basic state $(U^*(x^*, y^*), V^*(x^*, y^*))$ is solution of the boundary-layer equations along a flat plate in the absence of a pressure gradient and hence the interface remains flat. The computational domain in the streamwise direction is $x_a^* \leqslant x^* \leqslant x_b^*$. The velocity at infinity U_∞^* is used as reference velocity and the displacement thickness $\delta_a^* = \gamma\sqrt{\nu^* x_a^*/U_\infty^*}$, $\gamma = 1.7208$, at in-flow is the reference length. The Reynolds number is defined with the displacement thickness at in-flow

$$Re = \frac{U_\infty^* \delta_a^*}{\nu^*}. \tag{1}$$

When the wall is compliant the dimensionless vertical displacement $\eta(x, t)$ is solution of the dynamical equation

$$m\frac{\partial^2\eta}{\partial t^2} + d\frac{\partial\eta}{\partial t} + B\frac{\partial^4\eta}{\partial x^4} + \kappa\eta = [-p + \sigma](x, \eta). \tag{2}$$

Here p is the dimensionless perturbation fluid pressure and σ is the normal viscous stress of the perturbation fluid velocity with

$$\sigma = \frac{2}{Re}\left(\frac{\partial u}{\partial x}n_1^2 + \left(\frac{\partial u}{\partial y} + \frac{\partial v}{\partial x}\right)n_1 n_2 + \frac{\partial v}{\partial y}n_2^2\right), \tag{3}$$

(u, v) being respectively the streamwise and the wall-normal component of the disturbance flow velocity and $\vec{n} = (n_1, n_2) = \frac{1}{\sqrt{1+(\partial\eta/\partial x)^2}}(-\frac{\partial\eta}{\partial x}, 1)$ is the unit normal vector at the wall. The dimensionless coating parameters are such that

$$m = \frac{m^*}{\delta_a^*\rho^*}, \qquad d = \frac{d^*}{U_\infty^*\rho^*}, \qquad B = \frac{B^*}{\delta_a^{*3}\rho^* U_\infty^{*2}}, \qquad \kappa = \frac{\kappa^*\delta_a^*}{\rho^* U_\infty^{*2}}, \tag{4}$$

the coating characteristics m^*, d^*, B^* and κ^* being respectively the mass density per unit length, damping, flexural rigidity of the plate and spring stiffness. As usual the pressure is made dimensionless using $\rho^* U_\infty^{*2}$, ρ^* being the fluid density. The total fluid flow is governed by the Navier–Stokes system which has to be solved in the (unknown) domain

$$x_a \leqslant x \leqslant x_b, \qquad \eta(x, t) \leqslant y \leqslant \infty. \tag{5}$$

Only vertical displacements are allowed, hence the kinematical condition at the moving boundary writes

$$(U + u)\big[x, \eta(x, t)\big] = 0, \qquad \frac{\partial\eta}{\partial t} = (V + v)\big[x, \eta(x, t)\big]. \tag{6}$$

2.2. Numerical solution procedure

The geometry being an unknown of our problem, the physical domain (5) is transformed into a computational fixed domain using the mapping

$$t' = t, \qquad x' = x, \qquad y' = y - \eta(x, t). \tag{7}$$

The divergence operator, the Laplacien and the time derivative hence become

$$\vec{\nabla} = \vec{\nabla}' + \vec{D}(\eta), \qquad \Delta = \Delta' + L(\eta), \qquad \frac{\partial}{\partial t} = \frac{\partial}{\partial t'} + D_t(\eta) \tag{8}$$

with

$$\vec{D}(\eta) = \left(-\frac{\partial \eta}{\partial x'} \frac{\partial}{\partial y'}, 0 \right), \qquad D_t(\eta) = -\frac{\partial \eta}{\partial t'} \frac{\partial}{\partial y'}$$

and

$$L(\eta) = -\frac{\partial^2 \eta}{\partial x'^2} \frac{\partial}{\partial y'} - 2\frac{\partial \eta}{\partial x'} \frac{\partial^2}{\partial x' \partial y'} + \left(\frac{\partial \eta}{\partial x'} \right)^2 \frac{\partial^2}{\partial y'^2}.$$

The Navier–Stokes system is, written in terms of the disturbance flow velocity $\vec{u}$ and the disturbance pressure p,

$$\frac{\partial \vec{u}}{\partial t'} + G(\vec{u}) + N(\vec{u}) - \frac{1}{Re} \Delta' \vec{u} + \vec{\nabla}' p = S(\eta, \vec{u}, \vec{U}, p), \tag{9}$$

$$\vec{\nabla}' \cdot \vec{u} = -\vec{D}(\eta) \cdot \vec{U} - \vec{D}(\eta) \cdot \vec{u}, \tag{10}$$

where the gradient term $G(\vec{u})$ and the convective term $N(\vec{u})$ are $G(\vec{u}) = (\vec{U} \cdot \vec{\nabla}')\vec{u} + (\vec{u} \cdot \vec{\nabla}')\vec{U}$ and $N(\vec{u}) = (\vec{u} \cdot \vec{\nabla}')\vec{u}$. The right-hand side of equation (9) contains all the terms with η resulting from the mapping (7). In the computational frame (x', y') the kinematical conditions (6) and the boundary conditions at infinity for the disturbance velocity field are

$$\begin{aligned} &u(x', 0) = 0, \qquad \frac{\partial \eta}{\partial t'} = v(x', 0) \\ &\text{and} \quad p, u, v \to 0 \quad \text{as } y' \to \infty. \end{aligned} \tag{11}$$

For time-integration of equations (9)–(10) with (11), coupled to (2), second-order backward Euler differencing is used; the Cartesian part of the Laplacian as well as the pressure gradient are taken implicitly. An explicit second-order Adams–Bashforth scheme is used for the remaining terms. For the space-discretization, fourth-order central finite differences are used for the second derivatives in the streamwise x'-direction. In the wall-normal y'-direction Chebychev-collocation is used. For this purpose an algebraic mapping transforms the unbounded domain $0 \leqslant y' \leqslant \infty$ into the finite domain $\xi \in [-1, 1]$. A Poisson equation is solved for the pressure together with a Dirichlet-boundary condition ensuring a divergence-free velocity field. This is achieved using an influence matrix technique. In order to avoid oscillations at out-flow, a buffer domain is inserted between the physical domain and the out-flow boundary (Wiplier and Ehrenstein [17]).

3. Spring-backed elastic plate of finite length

3.1. Linear stability analysis

Despite the numerous linear parallel stability analyses available, we briefly review the different modes of instability which may arise in a boundary-layer flow with compliant coatings. The description of the different instability mechanisms will then provide a support for the interpretation of numerical simulation results to be discussed in the next section.

Linearizing the Navier–Stokes system (9) (by dropping the convective term $N(\vec{u})$ in (9) for a parallel basic state $\vec{U} = (U(y), 0)$) coupled to the kinematical conditions and to the dynamical equation, a normal-mode analysis, writing

$$\vec{u} = \big(\hat{u}(y), \hat{v}(y)\big)\mathrm{e}^{i(\alpha x-\omega t)}, \qquad p = \hat{p}(y)\mathrm{e}^{i(\alpha x-\omega t)}, \qquad \eta = \hat{\eta}\mathrm{e}^{i(\alpha x-\omega t)}, \tag{12}$$

leads to an eigenvalue problem via the dispersion relation

$$D(\omega, \alpha) = 0. \tag{13}$$

In a temporal stability analysis, the complex frequency $\omega = \omega_r + i\omega_i$ is computed as function of the (real) wavenumber α. Boundary-layer flows (with rigid walls) are known to be spatially (convectively) unstable, and performing a spatial stability analysis the complex wavenumber $\alpha = \alpha_r + i\alpha_i$ is computed as function of the real frequency ω. In the following the numerical solution procedure used to compute alternatively $\omega(\alpha)$ or $\alpha(\omega)$ is briefly summarized. Injecting the normal modes in the linearized Navier–Stokes system coupled to the dynamical equation, the frequency ω appears quadratically in the dynamical equation whereas the wavenumber α appears at the power of four in the dynamical equation and quadratically in the Navier–Stokes system.

The nonlinearities in frequency and wavenumber are linearized using auxiliary functions. The normal modes and the auxiliary functions once discretized using Chebyshev-collocation, one may formally introduce the vector

$$\Phi = \big(\varphi(y_1), \varphi(y_2), \ldots, \varphi(y_n), \eta, \alpha\hat{\eta}, \alpha^2\hat{\eta}, \alpha^3\hat{\eta}, \omega\hat{\eta}\big) \quad \text{with } \varphi = (\hat{u}, \hat{v}, \hat{p}, \alpha\hat{u}, \alpha\hat{v})$$

(y_i being the collocation points) which is solution of

$$(\alpha\mathbf{A} + \omega\mathbf{B} + \mathbf{C})\Phi = 0, \quad \text{hence} \quad D(\omega, \alpha) = \det(\alpha\mathbf{A} + \omega\mathbf{B} + \mathbf{C}) = 0 \tag{14}$$

for matrices **A**, **B**, **C**, derived from the discretization of the linearized Navier–Stokes system (together with the kinematical conditions and the dynamical equation) as well as from the relationships between the normal modes and the auxiliary functions. This procedure is known as the companion matrix method (Bridges and Morris [18]). Fixing the wavenumber α the frequencies ω (or alternatively the wavenumbers α for fixed ω) may hence be computed as generalized matrix eigenvalues using a standard QZ algorithm.

For a general stability analysis one has to consider both complex frequencies and wavenumbers. Fixing for instance the imaginary part ω_i of the frequency, complex α may be computed by varying the real part ω_r. For sufficiently high values ω_i (above the maximum temporal amplification rate), the real axis in the complex α-plane will separate two families of solutions: branches α^+ located in the half-plane $\alpha_i > 0$, corresponding to perturbation propagating downstream, and branches α^- in the half-plane $\alpha_i < 0$, corresponding to upstream propagating perturbations. For a convectively unstable flow with amplified downstream propagating modes, for instance in boundary-layers, a member of the α^+ family will cross the real axis, for decreasing ω_i-values, i.e. by lowering the Laplace contour in the ω-plane. The flow is convectively unstable, if no intersection between branches occurs in the α-plane for $\omega_i \geqslant 0$ (Huerre and Monkewitz [8]) (and then one may indeed compute α as function of the real frequency ω).

As a representative example for an elastic coating a spring-backed elastic plate with an elastic modulus of $E = 0.5$ MN/m^2, spring stiffness $\kappa^* = 115$ MN/m^3, plate density $\rho_m = 946$ kg/m^3 and plate thickness $b^* = 2$ mm is considered (the fluid being water with $\nu^* = 1.37 \times 10^{-6}$ m^2/s at flow speed $U_\infty^* = 18$ m/s). For a fixed Reynolds number $Re = 1700$ the complex wavenumbers $\alpha(\omega)$ have been computed using the QZ algorithm, for the real frequency varying from $-0.4 \leqslant \omega \leqslant 0.4$. As shown in *figure 1* the spectrum $\alpha(\omega)$

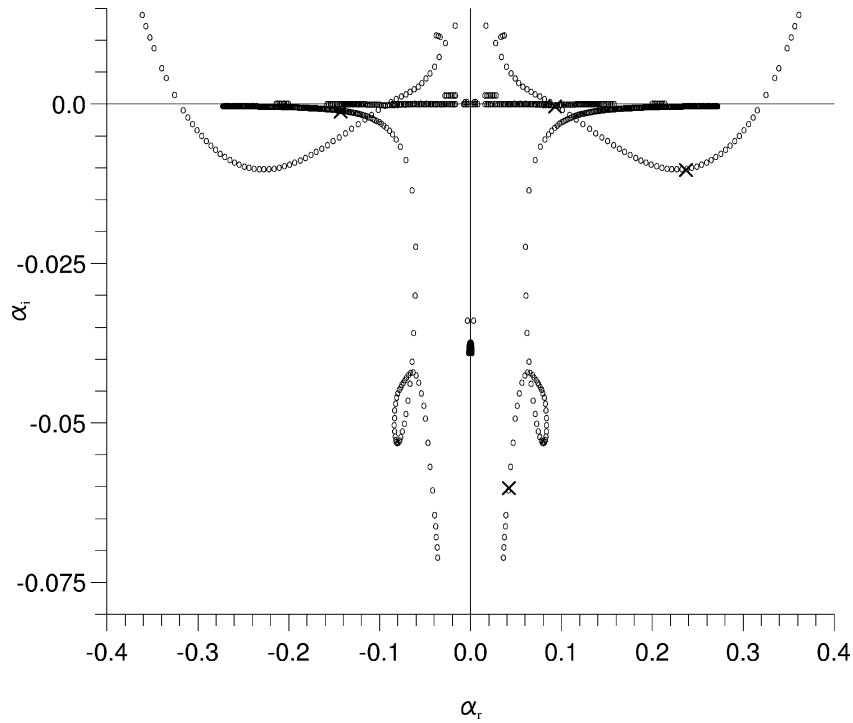

Figure 1. Global spectrum $\alpha(\omega)$, for a Blasius boundary-layer over a spring-baked elastic plate with elastic modulus $E = 0.5$ MN/m^2, spring stiffness $\kappa^* = 115$ MN/m^3 and plate thickness $b^* = 2$ mm at $Re = 1700$, for $-0.4 \leqslant \omega_r \leqslant 0.4$ ($\omega_i = 0$). $\times$ corresponds to modes for $\omega_r = 0.077554$, frequency used in the numerical simulation (cf. *figure 3*).

consists of several branches symmetric with respect to the imaginary axis in the complex α-plane. In this representation the different branches cross each other and it is not easy to detect the different roots $\alpha(\omega)$. Increasing ω_i-values and considering only positive real parts of the frequency (varying from $0 \leqslant \omega_r \leqslant 0.4$) the different branches may however be identified. *Figure 2* shows the results for fixed $\omega_i = 4 \times 10^{-3}$. One branch is just crossing the real axis and it corresponds to the Tollmien–Schlichting (TS) wave. For α_r in the vicinity of 0.1 and slightly above the real axis one detects a contour which corresponds to the travelling-wave flutter (TWF)-mode: for real frequencies above cut-off values, in the absence of fluid flow, free waves with real wavenumbers $\alpha = [(\omega^2 m - \kappa)/B]^{1/4}$ exist for the plate, which may easily be seen by considering the dynamical equation without damping and without second member. One distinguishes the corresponding branch in the global spectrum depicted in *figure 1* in the very vicinity of the real axis for $|\alpha_r| < 0.2$.

Besides the TS-branch as well as the TWF-branch, one retrieves the contour for the evanescent (E)-wave as well as the divergence (D)-wave, using a commonly used classification (cf. Carpenter [10]). These branches are located in the lower half of the complex α-plane and the corresponding perturbations are hence upstream modes. They are stable because the correponding α-roots do not cross the real axis in the α-plane, when lowering the Laplace contour. The divergence-wave mode is however almost neutral (though slightly damped) and a particular feature of the associated root is that it appears for negative α_r-values and the real part of the wave speed is hence negative.

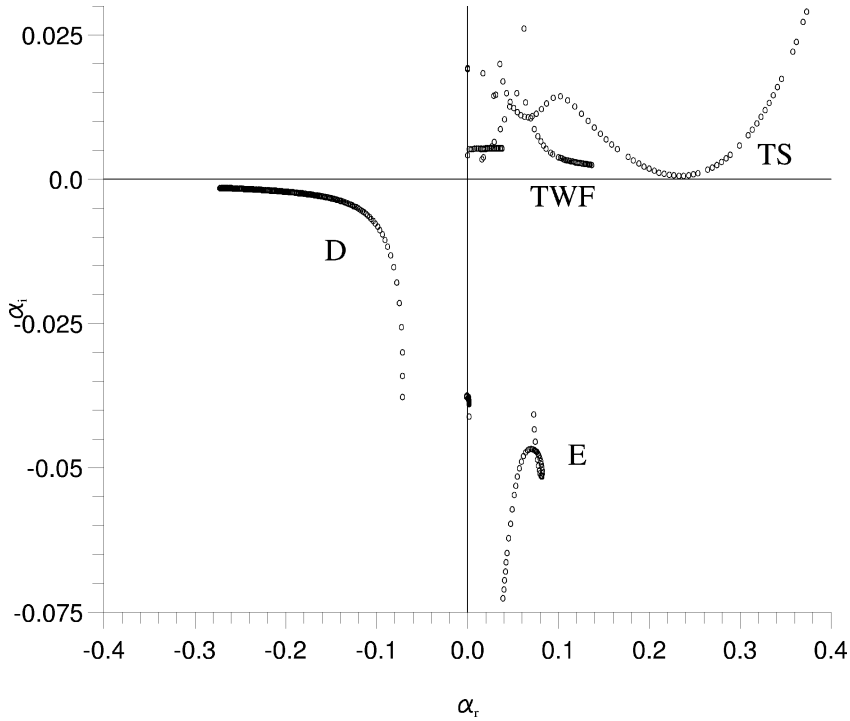

Figure 2. Global spectrum $\alpha(\omega)$, wall characteristics as in *figure 1*, at $Re = 1700$, for $\omega_i = 4 \times 10^{-3}$, $0 \leqslant \omega_r \leqslant 0.4$; TS: Tollmien–Schlichting mode, TWF: Travelling-Wave-Flutter, D: Divergence mode, E: Evanescent mode.

3.2. Spatial numerical simulation

Contrary to linear stability analyses which are based on the assumption of homogeneity in the streamwise direction, inhomogeneities and nonparallel effects may be considered when spatial numerical simulation is used. Nonparallel effects due to boundary-layer growth have been investigated for instance by Yeo et al. [6]. While modifying amplification rates (in particular for Reynolds numbers nearby criticality) boundary-layer growth is however not expected to affect the main features of the different instability mechanisms. Boundary-layer growth is easily taken into account when simulating the spatial evolution of disturbances in the boundary layer, but also inhomogeneities due to edge effects when using compliant panels of finite length. Finite-end effects are expected to be particularly important in the presence of downstream- and upstream-propagating waves.

In order to simulate the disturbance evolution in the global system, a spatial domain with an overall length of 24 TS-wavelengths (λ_{TS}) has been considered. The compliant panel has a length of $15\lambda_{TS}$, the leading edge being located at a distance of $3\lambda_{TS}$ from in-flow and adjacent to the trailing edge there is again a rigid plate of $6\lambda_{TS}$. Clamped-end conditions have been used for the compliant panel. Injecting a time-periodic perturbation at in-flow with frequency $\omega_r = 0.077554$ (the corresponding wavenumbers are marked as crosses in *figure 1*), the flow-perturbation being the eigenmode for a rigid plate at in-flow Reynolds number $Re = 1700$, the spatial evolution of the instability has been computed, solving the Navier–Stokes system coupled to the dynamical equation. (The computations have been performed using 20 points per Tollmien–Schlichting wavelength in x and 60 collocation points in y. For time-integration a time step of 0.1 has been used.) Similar simulations for a channel flow with compliant coatings of finite length, for the linearized Navier–Stokes system, have been reported for instance by Davies and Carpenter [19]. Spatially evolving disturbances, using time-periodic forcing

at in-flow, have also been described in Wiplier and Ehrenstein [17], for a boundary-layer flow with different compliant coatings.

The instantaneous wall displacement at $t = 27T$ (T being the time-period) is shown in *figure 3*, for a computation using the linearized (but nonparallel) Navier–Stokes system as well as for a full nonlinear computation, with a disturbance amplitude of $A = 0.001$ at in-flow. Several waves superimpose and the nonlinearities only slightly affect the wall displacement. The power spectrum of the instantaneous wall displacement shown in *figure 4* exhibits 4 wavenumbers: $\gamma_1 = 0.233$, $\gamma_2 = 0.096$, $\gamma_3 = 0.137$, $\gamma_4 = 0.0686$, corresponding approximately to the TS-instability, TWF-mode, divergence wave and evanescent wave, respectively, marked as crosses in *figure 1*. The divergence mode and evanescent mode are upstream propagating modes triggered by the trailing edge of the compliant panel.

According to the linear stability analysis results, the divergence instability appears as an almost neutral upstream propagating disturbance mode. To retrieve the corresponding panel response in the global system, the divergence wave has been triggered using an initial impulse-like flow perturbation. For this purpose the Navier–Stokes system has been integrated in time using a divergence-free Gaussian-type disturbance of the flow field

$$\begin{aligned} u &= -(y - y_0)\exp\left[-\frac{(x - x_0)^2}{2\sigma_x^2} - \frac{(y - y_0)^2}{2\sigma_y^2}\right], \\ v &= \frac{\sigma_y^2}{\sigma_x^2}(x - x_0)\exp\left[-\frac{(x - x_0)^2}{2\sigma_x^2} - \frac{(y - y_0)^2}{2\sigma_y^2}\right] \end{aligned} \tag{15}$$

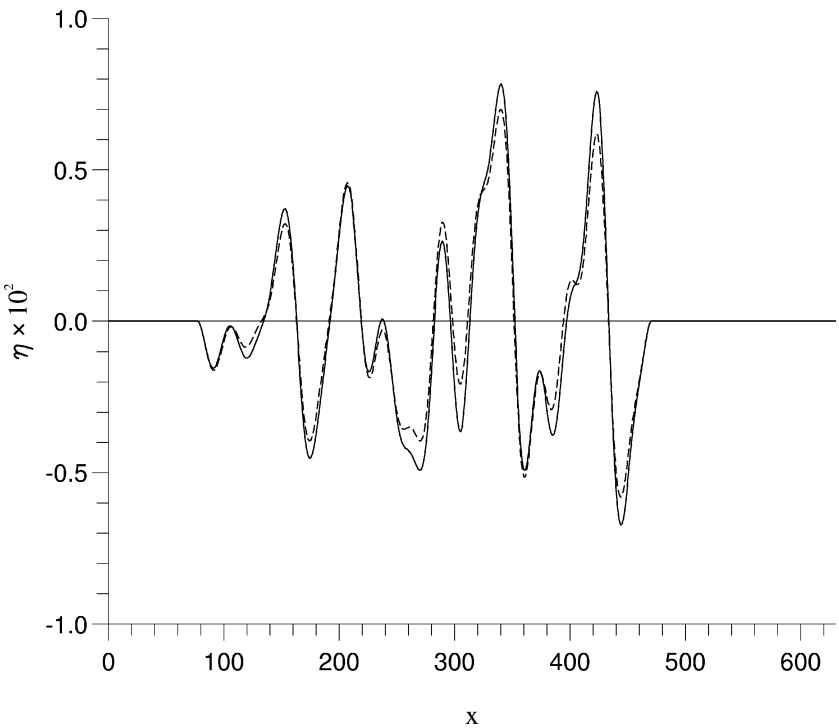

Figure 3. Elastic plate with thickness $b^* = 2$ mm, instantaneous wall displacement η at $t = 27T$ ($Re = 1700$) for in-flow perturbation with frequency $\omega_r = 0.077554$. —: nonlinear computation, initial amplitude $A = 0.001$; − − −: linear computation.

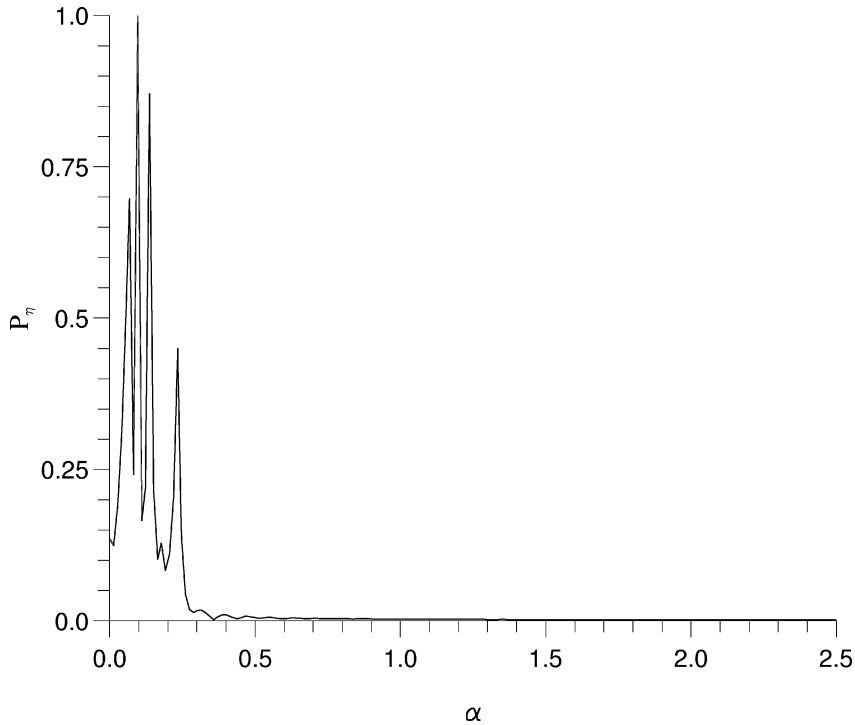

Figure 4. Elastic plate, power spectrum for wall displacement depicted in *figure 3* (for $A = 0.001$).

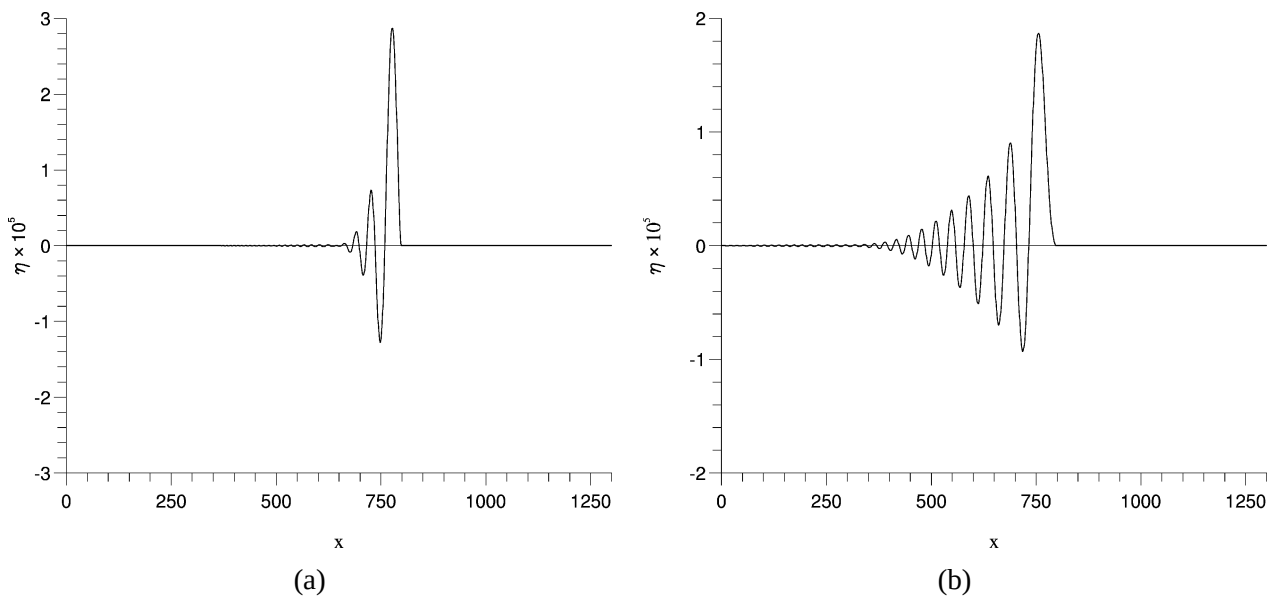

Figure 5. Wall displacement triggered by the divergence mode at the trailing edge $x = 800$ of the compliant coating, for $Re = 2000$, at (a) $t = 80$ and (b) $t = 200$.

as initial condition. This more or less (depending on σ_x, σ_y) spatially localized flow perturbation at $t = 0$ is suitable for the computation of the spatio-temporal evolution of wave packets and it has been used for instance by Delbende and Chomaz [20] for the analysis of convective and absolute instabilities in wakes. Here the perturbation with $\sigma_x = 2$ and $\sigma_y = 0.15$ in (15) is localized at $(x_0 = 800, y_0 = 1)$, that is at the trailing-edge of a compliant panel, ranging from $0 \leqslant x \leqslant 800$. The parameters of the compliant coating are the same as previously, the in-flow Reynolds number being now $Re = 2000$. (Note that for the present computation a parallel basic-flow has been considered.) The perturbation has been normalized such that the amplitude of the streamwise component is $A = 1 \times 10^{-3}$. The time evolution of the compliant coating is shown in *figure 5*. As expected, for increasing time the perturbation spreads upstream for a slowly decreasing amplitude at $x = 800$ (*figure 5(b)*), the divergence modes, interpreted as upstream propagating waves, being almost neutral.

4. Absolute instability

Linear stability analyses are again performed in order to detect parameter ranges in the wall parameters for the occurrence of an absolute instability behaviour in the boundary layer interacting with the elastic plate. Absolute instability behaviour may most likely be triggered by adding damping to the wall dynamics (Carpenter and Garrad [3]). Damping has a stabilizing effect on travelling-wave flutter, whereas the Tollmien–Schlichting mode is destabilized adding damping to the wall dynamics. Considering the same wall characteristics as in the previous section (elastic modulus $E = 0.5$ MN/m^2, spring stiffness $\kappa^* = 115$ MN/m^3, plate density $\rho_m = 946$ kg/m^3), but adding now a damping coefficient $d^* = 2000$ kg/m^{2}s, first a linear stability analysis has been performed using the parallel-flow assumption, for different plate thicknesses. Absolute instability occurs, if there is a merging for a positive imaginary part of ω_0 at a point (α_0, ω_0) between two spatial branches $\alpha^+(\omega)$ and $\alpha^-(\omega)$ which initially, for a Laplace contour with ω_i above the maximum temporal amplification rate, start on opposite sides of the real axis in the complex wavenumber plane. At this point, the deformed Fourier contour of integration is pinched (a recent review of the theory of absolute/convective instability and related topics may be found in Huerre and Rossi [21]). The pinch point corresponds to conditions $D(\alpha_0, \omega_0) = 0$, $\frac{\partial D}{\partial \alpha}(\alpha_0, \omega_0) = 0$ (or equivalently to saddle-points $\frac{\partial \omega}{\partial \alpha}(\alpha_0) = 0$ if one supposes that there is always a solution $\omega(\alpha)$ of the dispersion relation).

The Blasius-boundary layer with rigid walls is known to be convectively unstable and a complete analysis of the unstable wave packets based on the formal solution of the initial-boundary-value stability problem may be found in Brevdo [22]. Concerning the Blasius boundary layer with compliant coatings, damping has been recognized by Yeo et al. [14] to be responsible for the merging between a convectively unstable mode and an evanescent mode. For the damped plate with thickness $b^* = 0.8$ mm, at the Reynolds number $Re = 2000$, *figure 6(a)* shows the spatial branches in the region $(\alpha_r > 0, \alpha_i < 0)$ of the complex α-plane, function of ω, with $0 \leqslant \omega_r \leqslant 0.4$, for fixed $\omega_i = 12.5 \times 10^{-4}$. Only the Tollmien–Schlichting branch (depicted as small circles) has crossed the real axis. The evanescent-mode branch is depicted as crosses and is similar to the corresponding branch in *figure 2*. Decreasing the imaginary part of ω there is a pinch between these branches, as demonstrated in *figure 6(b)* and *6(c)*. The corresponding frequency and wavenumber are $\omega_0 = (0.108, 1.82 \times 10^{-3}), \alpha_0 = (0.18, -6.69 \times 10^{-2})$. Alternatively, as advocated for instance by Kupfer et al. [23], α_i-contours may be mapped in the complex ω-plane. This approach has for instance been used by Yeo et al. [14] for their analysis of absolute instability for an unstable boundary layer over viscoelastic walls. The α_i-contours in the ω-plane form indeed a cusp at ω_0, for the α_i-contour passing through α_0, as shown in *figure 7*. An upward vertical ray drawn from the cusp point intersects the $\alpha_i = 0$ contour only once, and hence there is only one crossing of the α_r-axis (for the root corresponding to the Tollmien–Schlichting wave) in the

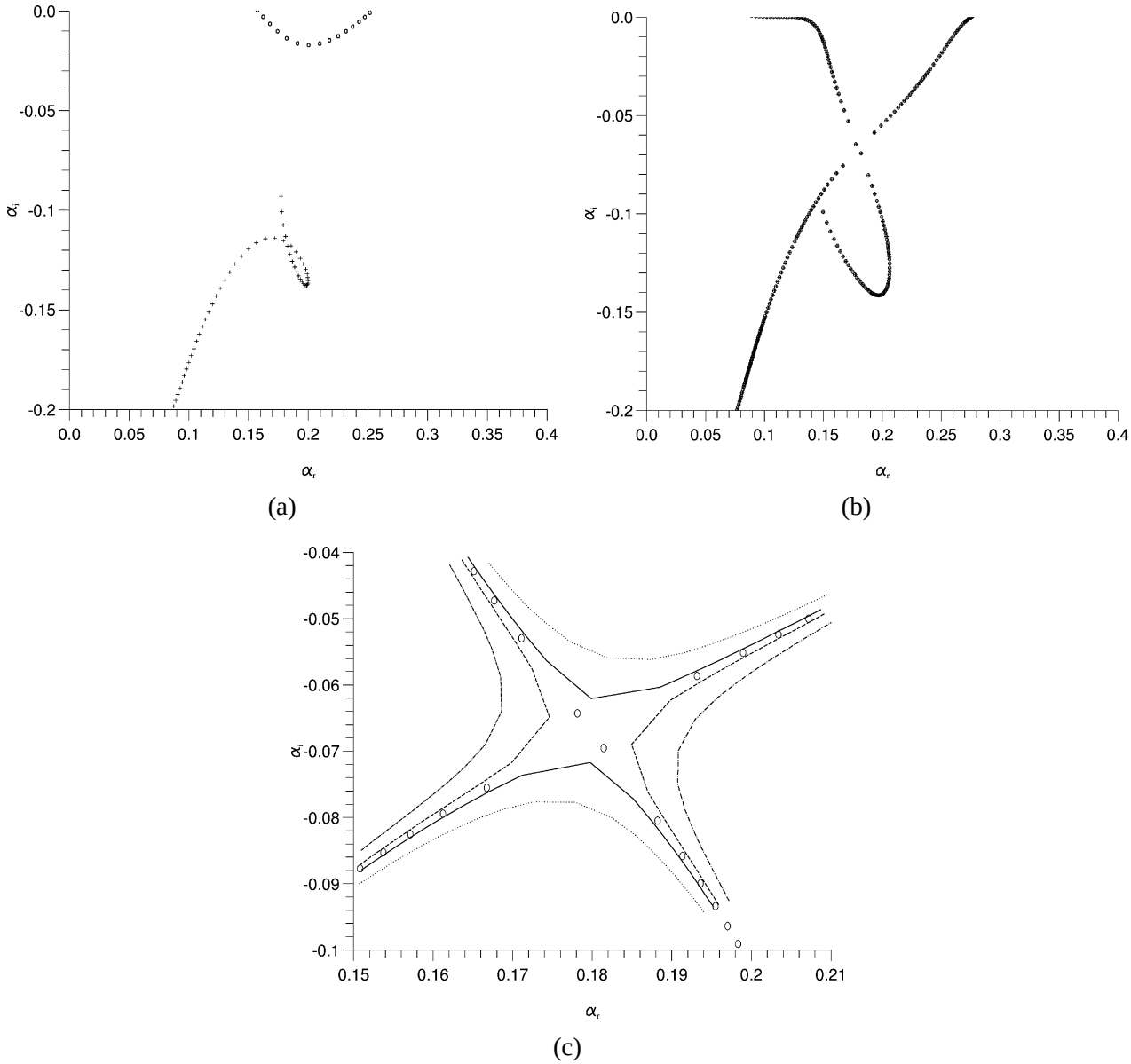

Figure 6. Global spectrum $\alpha(\omega)$, spring-backed plate with damping $d^* = 2000$ kg/m^{2}s and thickness $b^* = 0.8$ mm, at $Re = 2000$, for (a) $\omega_i = 12.5 \times 10^{-3}$ ($0 \leqslant \omega_r \leqslant 0.4$); ∘ Tollmien–Schlichting branch. + evanescent wave branch. (b) Merging between TS-branch and E-branch, at $\omega_i = 1.8 \times 10^{-3}$. (c) Branches in the vicinity of pinch point: $\cdots$ $\omega_i = 2.3 \times 10^{-3}$, — $\omega_i = 1.9 \times 10^{-3}$, ∘ $\omega_i = 1.8 \times 10^{-3}$, − − − $\omega_i = 1.7 \times 10^{-3}$ and − · − $\omega_i = 1.3 \times 10^{-3}$.

α-plane. Indeed, every crossing of α-roots in the α-plane when lowering the Laplace contour corresponds to an intersection of the vertical ray emanating from the cusp in the ω-plane with the $\alpha_i = 0$-contour (cf. [14,23]).

The imaginary part of ω at the cusp in the ω-plane (or alternatively at the pinch point in the α-plane) is positive and hence the instability is of absolute type. The pinch points have been computed for different Reynolds numbers. The corresponding absolute growth rates ω_i^a are shown in *figure 8*. For a plate thickness of $b^* = 0.8$ mm the fluid-structure system is absolutely unstable for a large parameter range in Reynolds number. While it was possible to compute a critical upper Reynolds number for absolute instability, the numerical

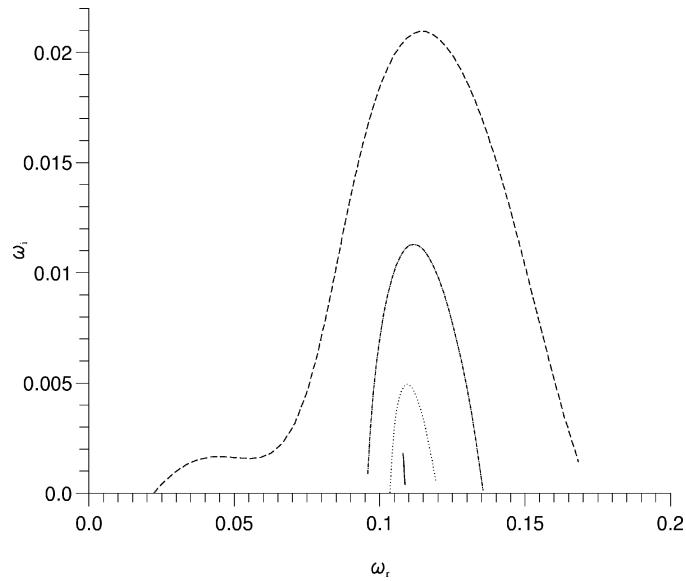

Figure 7. The α_i-contours in the complex ω-plane, same parameter values as in *figure 6*. - - - $\alpha_i = 0$; -.-.- $\alpha_i = -0.02$; ... $\alpha_i = -0.04$; cusp at $\alpha_i = -0.067$, it corresponds to intersection point in *figure 6(c)*.

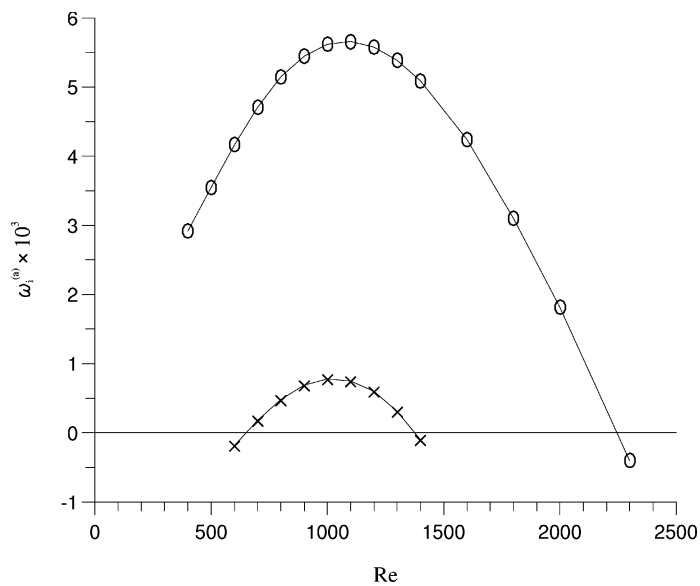

Figure 8. Absolute growth rate $\omega_i^{(a)}$ as function of Reynolds number Re, plate with damping $d^* = 2000$ kg/m^{2}s and thickness: $\circ$ $b^* = 0.80$ mm; $\times$ $b^* = 1.00$ mm.

procedure did not detect a critical lower Reynolds number. Increasing the plate thickness, the absolute growth rates decrease. Whereas there is still a parameter range of absolute instability for $b^* = 1$ mm, the fluid-structure system will become convectively unstable for somewhat thicker plates. We again emphasize that in the present case the absolute instability results from the merging between the Tollmien–Schlichting-mode and the evanescent mode. The travelling-wave-flutter mode is stable due to the damping.

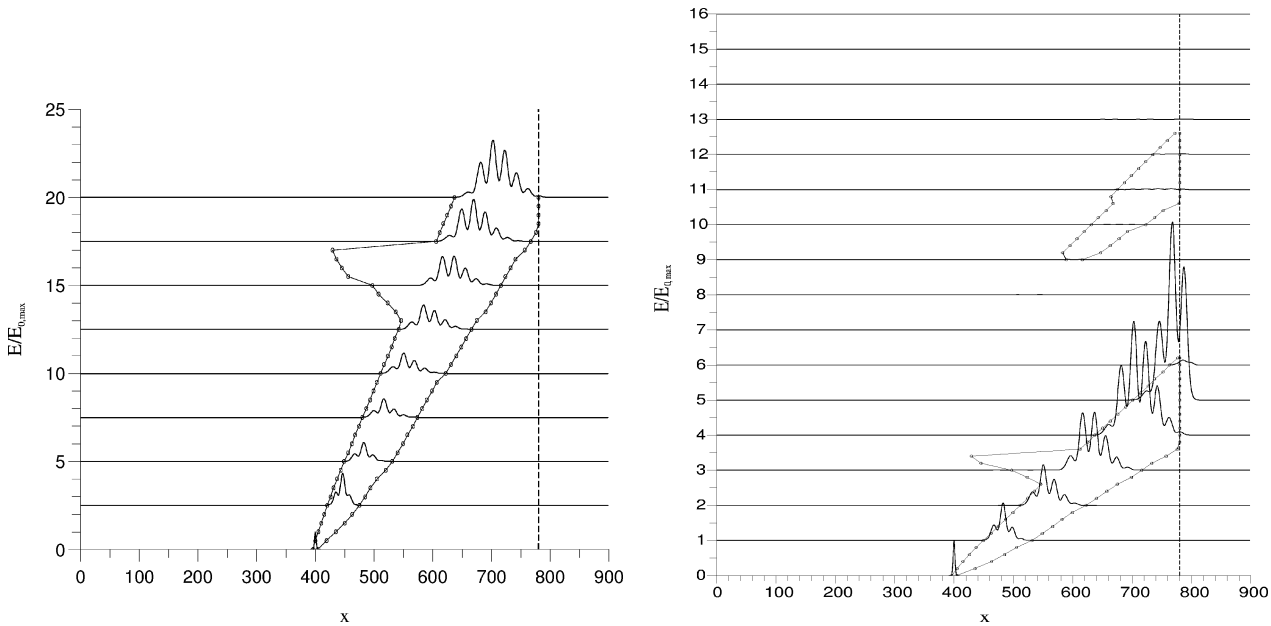

Figure 9. Evolution of normalized energy $E(x,t)/E_{0,\max}$ at (a) $t = 0, 100, 200, \ldots, 800$, at $Re = 1000$, for plate thickness $b^* = 2$ mm. ○: leading and trailing edges of wave packet. − − −: end of physical domain. (b) Normalized energy at $t = 0, 200, 400, \ldots, 3200$ with second convected wave packet starting at $t = 1800$.

In order to reinforce the findings on absolute instability based on the local linear stability analyses using the parallel-flow assumption, the spatial evolution of an initially localized perturbation has been computed solving the complete Navier–Stokes system coupled to the dynamical model (taking into account the spatial development of the basic flow as well as panel edge effects), for the same parameter values of the elastic plate. The compliant panel of finite length ranges from $200 \leqslant x \leqslant 600$. The perturbation with $\sigma_x = 2$ and $\sigma_y = 0.15$ in (15) is localized at $(x_0 = 400, y_0 = 1)$, that is one displacement thickness above the centre of the compliant panel. The overall length of the computational domain in x is 900 and 900 points have been used for discretization in x, whereas 40 collocation points have been considered in y. The timestep for time integration is $\Delta t = 0.1$. For this and the subsequent computations the perturbation has been normalized such that the amplitude of the streamwise component is $A = 1 \times 10^{-4}$. Even though nonlinearities are taken into account in the numerical model, we focus in the present computations on global, nonparallel effects and a rather low initial perturbation amplitude has been considered.

The energy $E(x,t) = \int_0^\infty (u^2 + v^2)(x, y, t)\mathrm{d}y$ has been chosen to represent the evolution of the wave packet in the (x,t)-plane. One computation for a plate thickness $b^* = 2$ mm is shown in *figure 9(a)*, the Reynolds number being $Re = 1000$. The small circles represent the numerically computed leading and trailing edges of the wave packet: upstream of the left edge and downstream of the right edge the perturbation energy becomes negligible (with $\frac{E}{E_{0,\max}} \leqslant 3 \times 10^{-3}$, $E_{0,\max}$ being the maximum of the initial energy). For this plate thickness the flow is convectively unstable and indeed the perturbation is convected downstream. The cusp in the leading edge of the wave packet occurs when the perturbation reaches the trailing edge of the compliant panel (at $x = 600$), which has some upstream influence on the flow field before the perturbation is convected again. The intersections with the ordinate of the succesive energy graphs correspond to zero normalized energy. (That is, to recover the normalized energy amplitudes at the different times one has to substract the value at the intersection

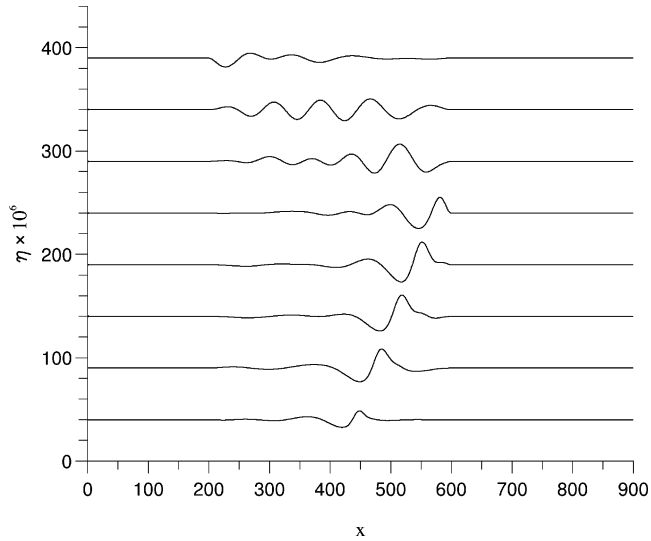

Figure 10. Evolution of wall displacement $\eta(x,t)$ at $t = 0, 100, 200, \ldots, 800$, at $Re = 1000$, $b^* = 2$ mm.

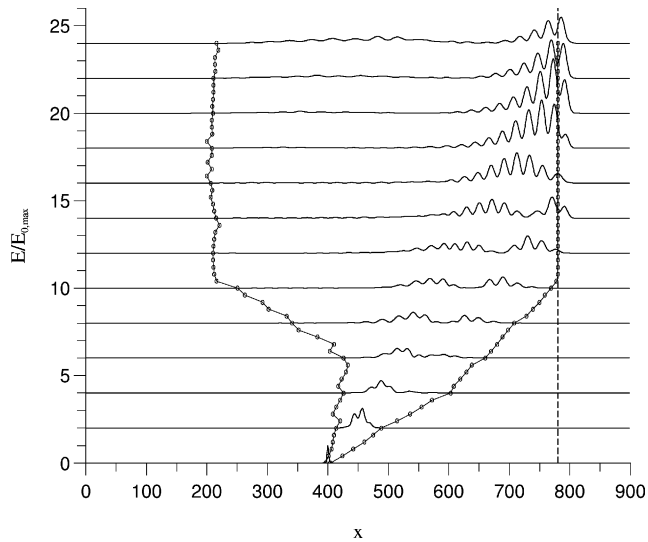

Figure 11. Evolution of normalized energy $E(x,t)/E_{0,\max}$ at $t = 0, 125, 250, \ldots, 1500$, at $Re = 1000$, $b^* = 1$ mm. ∘: leading and trailing edges of wave packet. − − −: end of physical domain.

of the different graphs with the ordinate.) Note that the buffer domain used to avoid reflections at the out-flow boundary (Wiplier and Ehrenstein [17]) starts at the vertical broken line in *figure 9(a)*.

In *figure 9(a)* the wave packet has not yet left the computational domain. The time integration has been pursued up to $t = 3200$ and indeed the wave packet leaves the domain, as shown in *figure 9(b)*. However, a second wave packet (with almost negligible amplitudes) appears for a later time. While the main disturbance is convected, the trailing edge triggers an upstream propagating (divergence-type) wall perturbation with decreasing amplitudes, which in turn, when reaching the leading edge of the plate, gives again rise to a convected wave packet in the boundary layer, but now with vanishing amplitudes. The behaviour of the wall displacement η is shown in *figure 10*. The perturbation in the wall is first convected, it reaches the trailing edge

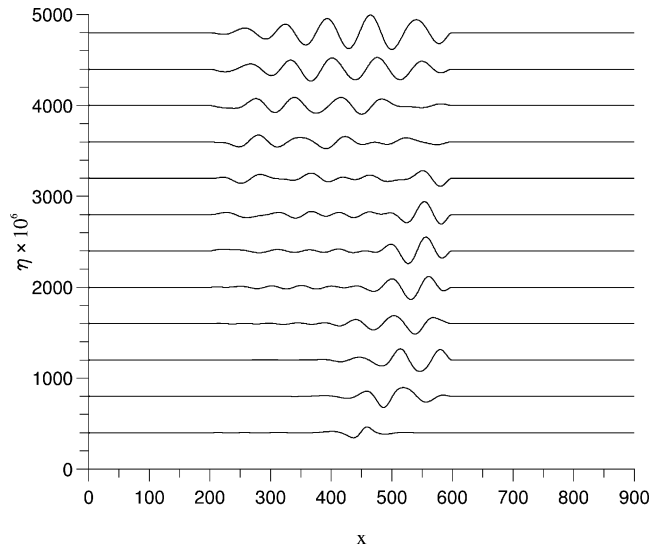

Figure 12. Evolution of wall displacement $\eta(x,t)$ at $t = 0, 125, 250, \ldots, 1500$, at $Re = 1000$, $b^* = 1$ mm.

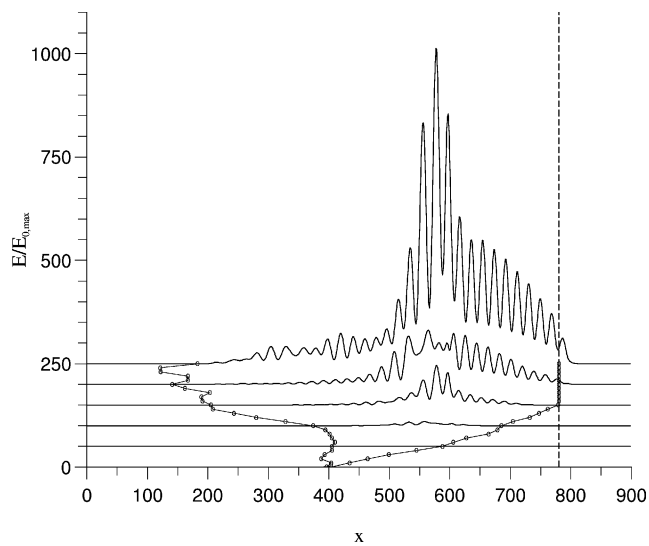

Figure 13. Evolution of normalized energy $E(x,t)/E_{0,\max}$ in the absolutely unstable case with $b^* = 0.8$ mm at $Re = 1000$, for $t = 0, 200, 400, \ldots, 1000$. ○: leading and trailing edges of wave packet. − − −: end of physical domain.

of the panel at $x = 600$, the wave is then reflected before it is progressively damped out. (Again, the intersection of the different graphs with the ordinate corresponds to zero wall displacement.)

The evanescent mode will be triggered when the perturbation reaches the trailing edge. When the system is absolutely unstable, the interaction with the oncoming travelling wave is expected to give rise to a perturbation which grows in time upstream and downstream from the source (that is the trailing edge). For a plate thickness of $b^* = 1$ mm, the local linear stability analysis predicts a weak absolute instability. Considering this plate thickness for the global computation with the in-flow Reynolds number $Re = 1000$, the evolution of the disturbance is shown in *figure 11*. The criterion used to compute the edges of the wave packet predicts an

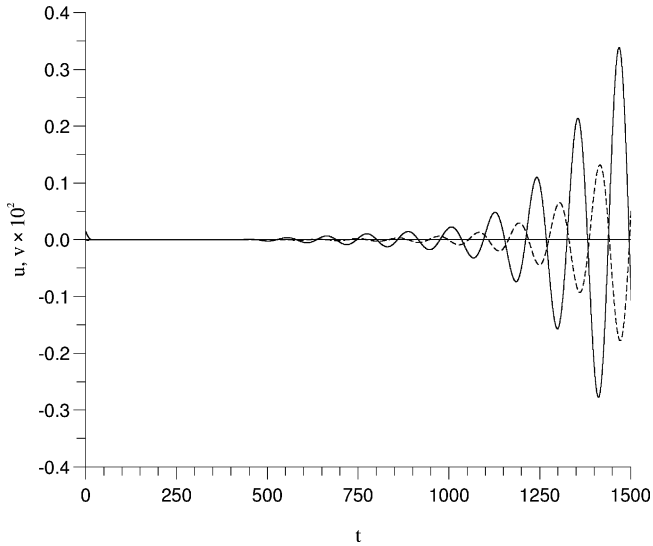

Figure 14. ——: streamwise component u and − − − wall-normal component v at $x = 400$, $y = 1$, as function of time, for $u = 10^{-4}$ at $t = 0$. Plate with thickness $b^* = 0.8$ mm, at $Re = 1000$.

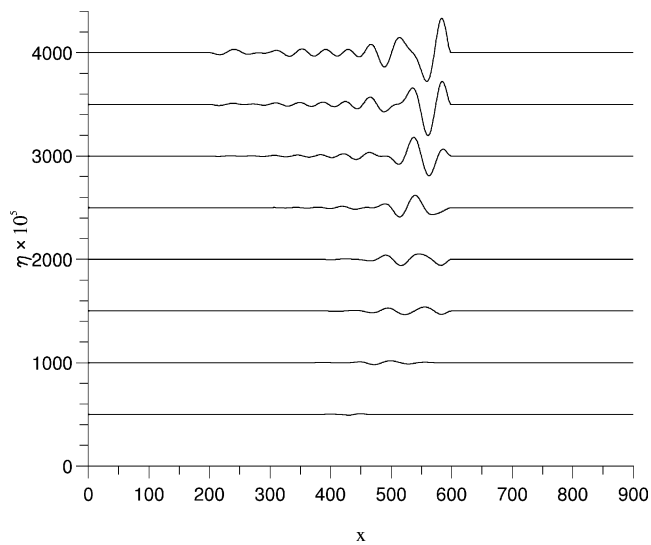

Figure 15. Wall displacement in the absolutely unstable case ($b^* = 0.8$ mm, at $Re = 1000$), for $t = 100, 200, 300, \ldots, 800$.

upstream propagating energy. However, a self-sustained instability mechanism typical for an absolute instability behaviour does not set in. The ambiguous global behaviour of the flow disturbance with regard to the local stability analysis may be due to nonparallelism. Also, nonlinearities may put a bound on the perturbation energy. While for this plate thickness of $b^* = 1$ mm the fluid flow appears to be at the margin of absolute instability, the wall displacement ultimately evolves into a temporally growing global mode due to wave reflections at the edges of the compliant panel, as shown in *figure 12*.

Finally, a plate thickness of $b^* = 0.8$ mm has been considered, for an in-flow Reynolds number of $Re = 1000$, this case being locally absolutely unstable with a fairly high absolute growth rate (cf. *figure 8*). The spatio-temporal diagram for the evolution of the flow-disturbance energy is shown in *figure 13*. In this case the flow is

clearly globally absolutely unstable. There is a dramatic increase in disturbance energy when the wave packet reaches the trailing edge of the compliant panel at $x = 600$. The time evolution of both streamwise and wall-normal disturbance flow components for a location above the centre of the compliant panel (at $x = 400$ and $y = 1$) is shown in *figure 14*, which illustrates the self-sustained oscillation mechanism. The signal periodically crosses the zero line and a Fourier analysis gives a frequency of $\omega_r \approx 0.054$. The local stability analysis predicts a pinch point (for a plate thickness of $b^* = 0.8$ mm and $Re = 1000$) for a complex frequency with $\omega_r = 0.0526$ and an absolute growth rate $\omega_i = 5.53 \times 10^{-3}$. Hence, the real parts of the frequencies given by both the local and global analyses compare quite well. Finally, *figure 15* shows the spatio-temporal evolution of the wall displacement. Here, in contrast to the case with $b^* = 1$ mm shown in *figure 12*, the maximum of the wall displacement remains located in the vicinity of the trailing edge.

5. Concluding remarks

By performing a local linear spatio-temporal stability analysis for an example of a damped, spring-backed elastic plate, the existence of a local absolute instability behaviour has been demonstrated, for sufficiently thin plates. It has been shown that pinching occurs via merging between the evanescent mode and the travelling-wave-type Tollmien–Schlichting mode.

In order to see whether the predicted behaviour may be retrieved for the global, nonparallel Navier–Stokes system coupled to the wall model, the fluid-structure system has been solved for a spatially localized Gaussian-type initial flow disturbance. These simulations are complementary to those reported in Lucey and Carpenter [11], who computed the interaction between an unsteady potential flow and a compliant coating. The results reported in the present work indicate that the divergence-type instability behaviour observed by Lucey and Carpenter is in fact due to the interaction between the stable, upstream propagating evanescent wave mode and a convectively unstable travelling wave, as suggested by Yeo et al. [14]. In the numerical simulations of the disturbance evolution, the absolute instability behaviour is triggered at the trailing edge of the finite compliant panel.

Our numerical experiments indicate that the global system with nonparallelism and panel-end effects behaves qualitatively, with regard to convective versus absolute instability, as predicted by the local linear stability analysis. Indeed, when the local linear stability behaviour predicts a convective instability, the disturbance in the flow is also convected in the global system, although the wall may exhibit a global deformation due to finite-end effects and mode reflections. On the other hand, the trailing edge is the source of disturbances spreading upstream and downstream in the flow for the global system for parameter ranges, where the system is absolutely unstable according to linear parallel stability theory. Hence, the sharp inhomogeneity at the trailing edge appears to play a similar role as a Dirac-type initial disturbance, used as a theoretical concept for triggering the entire wave packet in an infinitely extended system.

References

[1] Gad-el-Hak M., Compliant coatings: a decade of progress, Appl. Mech. Rev. 49 (1996) S147–S157.
[2] Carpenter P.W., Garrad A.D., The hydrodynamic stability of flow over Kramer-type compliant surfaces: Part 1. Tollmien–Schlichting instabilities, J. Fluid Mech. 155 (1985) 465–510.
[3] Carpenter P.W., Garrad A.D., The hydrodynamic stability of flow over Kramer-type compliant surfaces: Part 2. Flow-induced surface instabilities, J. Fluid Mech. 170 (1986) 199–232.
[4] Joslin R.D., Morris P.J., The sensivity of flow and surface instabilities in boundary-layer transition, J. Fluid Struct. 3 (1989) 423–437.
[5] Joslin R.D., Morris P.J., Effect of compliant walls on secondary instabilities in boundary-layer transition, AIAA J. 30 (1992) 332–339.
[6] Yeo K.S., Khoo B.C., Chong W.K., The linear stability of boundary-layer flow over compliant walls: effects of boundary-layer growth, J. Fluid Mech. 280 (1994) 199–225.

[7] Ehrenstein U., Rossi M., Nonlinear Tollmien–Schlichting waves for a Blasius flow over compliant walls, Phys. Fluids 8 (1996) 1036–1051.
[8] Huerre P., Monkewitz P.A., Local and global instabilities in spatially developing flows, Ann. Rev. Fluid Mech. 22 (1990) 473–537.
[9] Brazier-Smith P., Scott J., Stability of fluid flow in the presence of a compliant surface, Wave Motion 6 (1984) 574–560.
[10] Carpenter P.W., Status of transition delay using compliant walls, in: Bushnell D.M., Hefer J.F. (Eds.), Viscous Drag Reduction in Boundary-Layers, Progress in Astronautics and Aeronautics 123, 1990, pp. 79–113.
[11] Lucey A.D., Carpenter P.W., A numerical simulation of the interaction of a compliant wall and inviscid flow, J. Fluid Mech. 234 (1992) 121–146.
[12] Lingwood R.J., Peake N., On the causal behaviour of flow over an elastic wall, J. Fluid Mech. 396 (1999) 319–344.
[13] Crighton D., Oswell J.E., Fluid loading with mean flow. I. Response of an elastic plate to localized excitation, Philos. T. Roy. Soc. A 335 (1991) 557–592.
[14] Yeo K.S., Khoo B.C., Zhao H.Z., The absolute instability of boundary-layer flow over viscoelastic walls, Theor. Comput. Fluid Dyn. 8 (1996) 237–252.
[15] Cooper A.J., Carpenter P.W., The stability of rotating-disc boundary-layer flow over a compliant wall. Part 2. Absolute instability, J. Fluid Mech. 350 (1997) 261–270.
[16] de Langre E., Ouvrard A.E., Absolute and convective bending instabilities in fluid-conveying pipes, J. Fluid Struct. 13 (1999) 663–680.
[17] Wiplier O., Ehrenstein U., Numerical simulation of linear and nonlinear disturbance evolution in a boundary layer with compliant walls, J. Fluid Struct. 14 (2000) 157–182.
[18] Bridges T.J., Morris P.J., Differential eigenvalue problems in which the parameter appears nonlinearly, J. Comp. Phys. 55 (1984) 437–460.
[19] Davies C., Carpenter P.W., Instabilities in a plane channel flow between compliant walls, J. Fluid Mech. 352 (1997) 205–243.
[20] Delbende I., Chomaz J.-M., Nonlinear convective/absolute instabilities in parallel two-dimensional wakes, Phys. Fluids 10 (1998) 2724–2736.
[21] Huerre P., Rossi M., Hydrodynamic instabilities in open flows, in: Gadrèche C., Manneville P. (Eds.), Hydrodynamic and Nonlinear Instabilities, Cambridge University Press, Cambridge (UK), 1998, pp. 81–294.
[22] Brevdo L., Convectively unstable wave packets in the Blasius boundary layer, Z. Angew. Math. Mech. 6 (1995) 423–436.
[23] Kupfer K., Bers A., Ram A.K., The cusp map in the complex-frequency plane for absolute instabilities, Phys. Fluids 30 (1987) 3075–3082.